Preparation of carbon spheres/lignin materials and adsorption of toxic metal ions

Nannan Zhang[a], Jie Pan[b], Fulong Cheng[b],*

[a]*Modern Experiment Center, Harbin Normal University, Harbin 150025, China, email: nnz_wabb@163.com*
[b]*Key Laboratory of Water Environment Evolution and Pollution Control in Three Gorges Reservoir, Chongqing Three Gorges University, Chongqing 404100, China, email: chengfltgu@126.com (F.L. Cheng), panjtgu@126.com (J. Pan)*

ABSTRACT

High adsorption capacity, fast adsorption kinetics, excellent reusability and low cost are highly demanded adsorbents used in the treatment of heavy metal ions. Carbon is prepared by one-step hydrothermal method and then combined with lignosulfonate to form a carbon-lignosulfonate adsorbent. Field-emission scanning electron microscope, Fourier-transform infrared spectrometer, X-ray diffractometer and Raman spectrometer are used to characterize and analyze the adsorbent. The effects of solution pH, initial concentration of heavy metal ions, time, temperature, and dose on the performance of adsorbents are discussed. The research found that when pH = 7, the dose reaches 0.01 g, the temperature is 25°C, and the heavy metal ion concentration is 40 mg L^{-1}, the adsorption time is 60 min, and the removal rate is close to 100%. Modeling the experimental data reveals that the pseudo-second-order kinetics and Langmuir isotherm are closer to the actual adsorption. The results reveal that the adsorption of Pb^{2+} and Cu^{2+} by carbon-lignosulfonate is spontaneous exothermic chemisorption. Simultaneously, the carbon-lignosulfonate adsorbent has good reusability, and the adsorption efficiency is still above 80% after 5 cycles. This work provides a new idea for the adsorption of toxic metal ions in an aqueous solution by lignosulfonate. This work provides a new idea for the adsorption of toxic metal ions in an aqueous solution by lignosulfonate.

Keywords: Carbon; Lignosulfonate; Adsorption; Heavy metal ion

1. Introduction

All life activities are inseparable from water. Although the earth's ocean area accounts for 71% of the total area, freshwater accounts for less than 3%, groundwater and polar glaciers account for 2.7%, and available freshwater resources are less than 0.1%. However, with the development of industry, the improper treatment of wastewater, and massive wastewater directly discharged into the environment, resulting in water pollution, especially the pollution of heavy metal ions [1–5]. Heavy metal ions cannot be degraded, and have strong toxicity, through the food chain enrichment, which will cause devastating damage to

humans [6,7]. The use of clean and reliable water is the minimum guarantee for people's life, so countries all over the world are looking for a way to solve the pollution problem of heavy metal ions.

Nowadays, the commonly used methods are extraction, ion exchange, membrane separation, and adsorption. Extraction, ion exchange and membrane separation have better removal properties, however, the high price and poor repeatability limit the application of these technologies. Adsorption has the advantages of simple operation, environmental protection and low cost, which has been widely studied to deal with the contamination of heavy

---

* Corresponding author.

metal ions. However, it is seen that most highly efficient adsorbents, such as activated carbon, covalent organic framework-based materials are expensive and have limited economic perspective. At present, the development trend of adsorbents is in the direction of green, efficient and economic materials [8–11].

Carbon is one of the most common elements in nature. It exists in the atmosphere, crust and biology in various forms, and is also an important part of life. There are many kinds of allotropic carbon in nature, such as diamond, graphite, graphene, carbon nanotubes, C60, hexagonal meteorite diamond (Lansdale). The special properties of carbon are widely used in adsorption materials, activated carbon and carbon nanotubes are commonly used adsorption materials. The adsorption capacity of activated carbon to treat heavy metal ions is large, but its disadvantages are high price, short service life and high operation cost. Heavy metal ions and activated carbon surface for ion exchange, to achieve the purpose of removal. Some scholars have found that –OH and –COOH on the surface of activated carbon can coordinate with ions, resulting in the deposition of ions on the surface of activated carbon. Hao et al. [12] treated poly((dimethylamino)ethyl methacrylate) with activated carbon made from rice husk to obtain PDMAEMA-RHC composite, which was used to treat copper ion. It was found that the pore size of the PDMAEMA-RHC adsorbent was 3.8 nm, the surface area was 789 $m^2 g^{-1}$, and the adsorption capacity for copper ion was 31 mg g^{-1}. Mustafa et al. [13] used zinc chloride to activate hazelnut shells and then put them into nitrogen to prepare activated carbon. Its surface area was 1,092 $m^2 g^{-1}$. The adsorption capacity of the adsorbent for the copper ion is 6.6 mg g^{-1}, and the adsorption capacity for the lead ion is 13.1 mg g^{-1}. A carbon nanotube is a kind of carbon material with small size, large specific surface area and high mechanical strength. Carbon nanotubes (CNTs) are cylindrical carbon tubes formed by the crimping of graphite sheets. The hollow and layered structure of MWCNTs makes it a good adsorbent. Li et al. [14] loaded Al_2O_3 on carbon nanotubes to form composite materials, which had a good effect on treating heavy metal ions, and its adsorption capacity for lead ion was 17.5 mg g^{-1}. Due to the excellent performance of carbon materials in adsorption, it has been a research hotspot for researchers to find low-cost and high-yield preparation methods. The preparation of carbon materials includes a solvent (hydrothermal) method, template method, vapor deposition method and emulsification method.

Hydrothermal carbon materials account for a large proportion of carbon adsorption materials. Hydrothermal carbon spheres were synthesized from biomass by the hydrothermal method [15,16]. In nature, lignin is the second-largest renewable resource after cellulose. It is estimated that about 6×10^{14} tons of lignin can be produced in the world every year. However, due to the complex amorphous structure of lignin, its industrial utilization is limited. At present, lignin mainly exists in papermaking wastewater and agricultural waste, and its utilization rate is very low [17–19]. The sulfite or bisulfate contained in the pulp waste liquid of the calcium bisulfite pulping method directly combines with the hydroxyl group in the lignin molecule to generate lignosulfonate [20–23]. The main industrial uses of quality sulfonates include concrete water reducing agent; binder for flotation and smelting of ore powder; dispersant and binder for refractory materials; reducing the carbon content in ceramics to improve green strength. Sodium lignosulfonate was prepared into hydrothermal carbon by the hydrothermal method. An enormous number of functional groups were introduced into the surface of sodium lignosulfonate, which enhanced its binding with other substances. This will greatly increase the application prospect of lignosulfonate [24–29].

In this paper, sodium lignosulfonate was used as a carbon source to synthesize hydrothermal carbon spheres, which were then combined with sodium lignosulfonate to form a modified lignosulfonate adsorbent. Heavy metal ions were treated by adsorbents, and their adsorption properties were evaluated by various characterization methods. Different factors were set up to evaluate the adsorption performance and adsorption mechanism of the adsorbent.

2. Experiment

2.1. Material

Sodium lignosulfonate (LS), cetyltrimethylammonium bromide (CTAB), HCl, ethanol, glutaraldehyde, triethylenetetramine, lead nitrate, copper nitrate are analytical grades, all from Shanghai Sinopharm Group Co., Ltd., (Shanghai, China).

2.2. Preparation of C-LS adsorbent

First, 30 mL concentrated hydrochloric acid was added to 30 mL deionized water while stirring, and 3 g sodium lignosulfonate was added into the solution. Next, add cetyltrimethylammonium bromide (CTAB) to the solution, stir until dissolved, and then transfer the solution to a 100 mL reaction kettle, and react at a constant temperature of 180°C for 12 h. After the reaction, the solid and liquid were separated by centrifuge, washed with deionized water and anhydrous ethanol until the washing solution was colorless, and then dried in an oven to obtain carbon materials. After drying, CTAB was removed from the carbon material by the tubular furnace (specific parameters: nitrogen protection, 5°C min heating rate increased from 25°C to 800°C), and then cleaned with deionized water, and finally dried to obtain hydrothermal carbon spheres.

100 mL deionized water, 4 g sodium lignosulfonate and 3 g carbon materials were added into a three-necked flask in turn and dispersed by ultrasonic wave. Then refluxing at 60°C for 60 min. 50 mL glutaraldehyde was continuously added to the above solution, and the reaction continued for 3 h. After the reaction was completed, it was filtered and washed to obtain a brown precipitate. Next, the brown solid, 6 mL triethylenetetramine and 100 mL deionized water were added into a three-necked flask in turn, ultrasonically dispersed, and refluxed in a water bath at 60°C for 30 min. 5 mL of glutaraldehyde was continuously added to the three-necked flask to react for 3 h. After the reaction was completed, the solid and liquid were separated by centrifuge, washed with deionized water until the

washing solution was colorless, and then dried in an oven to obtain carbon-coated modified sodium lignosulfonate (C-LS) [30]. The mechanism of the above experiment is shown in Fig. 1.

2.3. Adsorption properties of C-LS adsorbent

First of all, 1,000 mg L^{-1} Pb^{2+} and Cu^{2+} were prepared in a 1 L volumetric flask as the reserve for the adsorption experiment. A 50 mL beaker was added with metal ion solution and adsorbent, and the adsorption equilibrium was maintained at a constant temperature. When studying the influencing factors, the parameters are set as follows: pH 2–7, initial concentration 5–200 mg L^{-1}, adsorbent dosage 0.01–0.05 g, temperature 25°C–45°C, time 0–180 min. The ion concentration was measured by inductively coupled plasma (ICP-OES) and the adsorption capacity (q_e) was calculated by Eq. (1).

$$q_e = \frac{(C_0 - C_e)V}{w} \tag{1}$$

where C_0 is the initial concentration, C_e is the equilibrium concentration (mg L^{-1}), V is the solution volume (L), and w is the adsorbent weight (g). In order to control the directness, all adsorption experiments of this batch were conducted three times, and the average value was reported.

When studying the kinetic model, the parameters are set as follows: pH = 7, the metal ion concentration is 40 mg L^{-1}, the amount of adsorbent is 0.01 g, the adsorption time is 0–180 min, and the temperature is 25°C.

Pseudo-first-order model:

$$\ln(q_e - q_t) = \ln q_e - k_1 t \tag{2}$$

Pseudo-second-order model:

$$\frac{t}{q_t} = \frac{t}{k_2 q_e^2} + \frac{1}{q_e} \tag{3}$$

Intraparticle diffusion model:

$$q_t = k_p t^{1/2} + C \tag{4}$$

where k_1 (min^{-1}), k_2 (g mg^{-1} min^{-1}), and k_p (mg g^{-1} min$^{-1/2}$) are pseudo-first-order rate constants, pseudo-second-order rate constants, and intra-particle diffusion rate constants, respectively. t (min) is time, C is a constant, and q_t (mg g^{-1}) is the adsorption capacity corresponding to t.

When studying the isotherm model, the experimental parameters are set as follows: pH = 7, the metal ion concentration is 5–200 mg L^{-1}, the amount of adsorbent is 0.01 g, the adsorption time is 180 min, and the temperature is 25°C–45°C.

Langmuir adsorption isotherm:

$$\frac{C_e}{q_e} = \frac{C_e}{q_{m,L}} + \frac{1}{K_L q_{m,L}} \tag{5}$$

Freundlich adsorption isotherm:

$$\ln q_e = \ln K_F + \frac{1}{n}\ln C_e \tag{6}$$

where $q_{m,L}$ (mg g^{-1}) is the maximum saturated adsorption capacity. K_L (L mg^{-1}) is the Langmuir adsorption constant related to the adsorption energy. K_F (L g^{-1}) is the Freundlich adsorption constant related to the adsorption capacity, and n is the constant.

When discussing thermodynamics, the experimental parameters were set as follows: pH = 7, metal ion concentration 40 mg L^{-1}, adsorbent dosage 0.01 g, adsorption time 180 min, and temperature 25°C–45°C.

$$\Delta G^\circ = \Delta H^\circ - T\Delta S^\circ \tag{7}$$

$$\ln\left(\frac{q_e}{C_e}\right) = \frac{\Delta S^\circ}{R} - \frac{\Delta H^\circ}{RT} \tag{8}$$
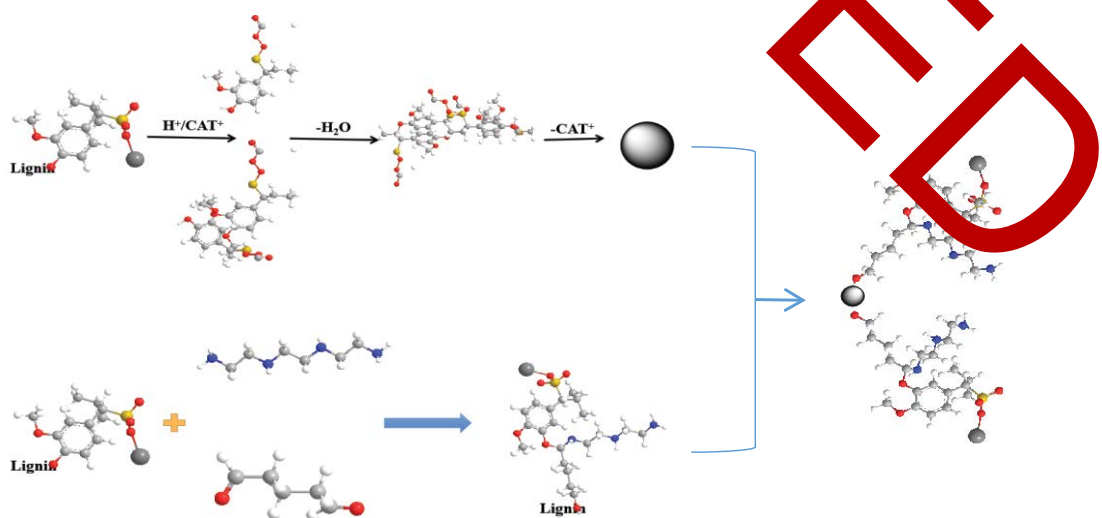
Fig. 1. Schematic diagram of C-LS synthesis mechanism.

where $\Delta G°$ (kJ mol^{-1}) is Gibb's free energy; $\Delta S°$ (J mol^{-1} K^{-1}) is adsorption entropy change; $\Delta H°$ (kJ mol^{-1}) is adsorption enthalpy change; R is the universal gas constant.

2.4. Characterization of C-LS absorbent

The spherical structure of carbon spheres and the appearance structure of C-LS adsorbent were studied by scanning electron microscopy (SEM, FEI Quanta 200, Netherlands). The functional groups of sodium lignosulfonate and C-LS adsorbent were characterized by Fourier-transform infrared spectroscopy FTIR (Nicolet 5700, US). The elemental content of the sample was characterized and analyzed with an Element Analyzer (PerkinElmer 2400II, Japan). The phases of carbon spheres and C-LS adsorbent were characterized and analyzed by a X-ray crystal analyzer (TDF-3200, China). The composition of the carbon sphere and C-LS adsorbent was characterized and analyzed by Raman spectrometer (ATC0400-UV, Japan).

3. Results and discussion

Fig. 2 shows the scanning electron micrograph of hydrothermal carbon spheres and C-LS adsorbent and C-LS adsorbent mapping. Fig. 2A shows that the hydrothermal carbon sphere is a kind of sphere, and the carbon

sphere exhibits an agglomeration phenomenon, shaped like a grape. The diameter of these carbon spheres is about 1–2 µm, and the surface is smooth, which shows that sodium lignosulfonate successfully synthesized hydrothermal carbon spheres. Fig. 2B shows that the surface of C-LS is uneven, showing a stacking phenomenon. Careful observation reveals that the surface of C-LS has holes and many folds, which provides more surface area and is more conducive to the adsorption of heavy metal ions. The mapping diagram contains C, N, O, S, and Na elements, which also proves the successful synthesis of the C-LS adsorbent.

Fig. 3A is the infrared spectra of sodium lignosulfonate (LS) and C-LS adsorbent. It can be seen from the figure that at 3,400 cm^{-1}, both substances have O–H tensile vibration peaks; near 2,900 cm^{-1}, both substances have C–H tensile vibration peak; the aromatic ring C=C tensile vibration of sodium lignosulfonate appears near 1,450; 1,500 and 1,600 cm^{-1}; the adsorption peaks of the sulfonic acid group –SO$_3$ appeared in 1,200 and 1,040 cm^{-1} additives. It is revealed in Fig. 3A that the C-LS adsorbent has a characteristic peak of sodium lignosulfonate, and there is also the vibration of N–H at 1,660 cm^{-1}, and N–H out-of-plane bending vibration at 810 cm^{-1}. And the C–N tensile vibration at 1,280 cm^{-1}. The infrared spectra show that the sodium lignosulfonate combines with carbon and introduces an amino group.
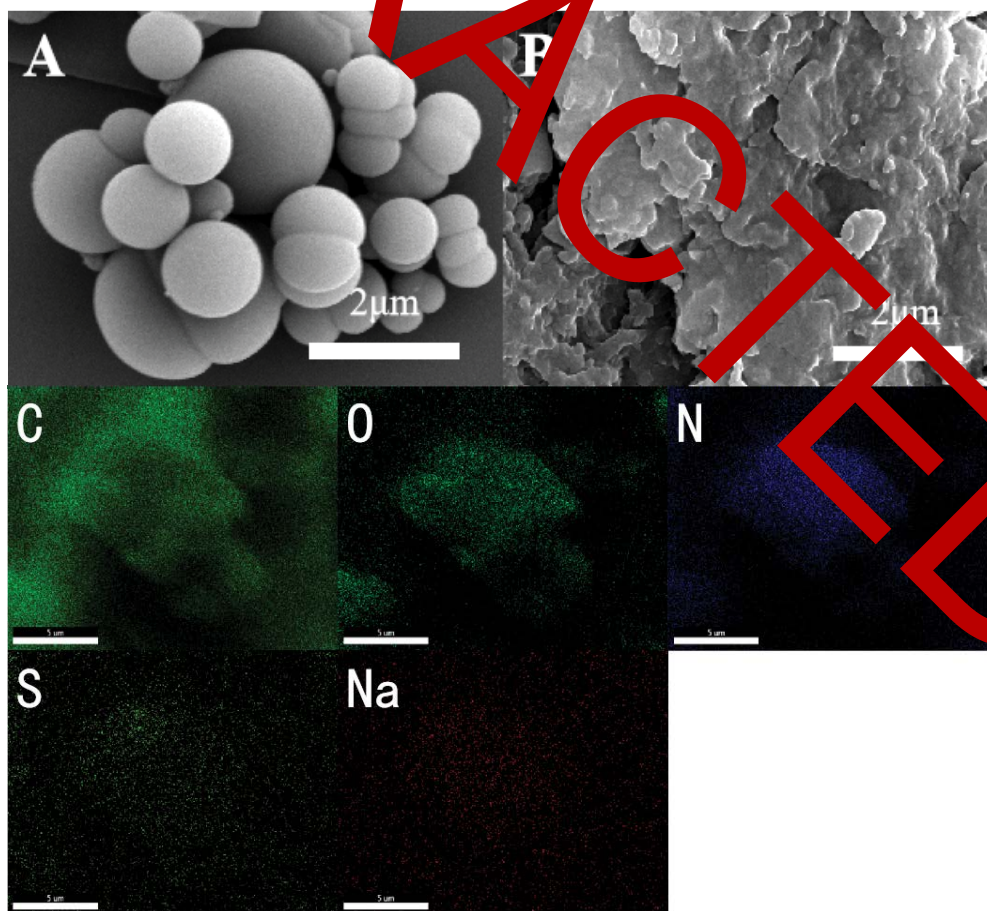
Fig. 2. SEM (Scanning electron micrograph) of carbon spheres and C-LS adsorbent, and mapping of C-LS adsorbent.

Fig. 3B is the X-ray diffraction (XRD) patterns of hydrothermal carbon spheres and C-LS adsorbent. It can be seen from the figure that both lines only show a large diffraction peak at 23°. The C-LS adsorbent has a carbon peak similar to hydrothermal carbon, indicating that sodium lignosulfonate and hydrothermal carbon succeeded combined, and the two substances did not form a crystal structure.

Both hydrothermal carbon and C-LS adsorbent are carbon materials, and Raman spectroscopy was used to characterize the properties of carbon materials. Fig. 3C is the Raman spectrum of hydrothermal carbon and C-LS adsorbent. There are two adsorption peaks in the Raman diagram, the peak on the left is the D-band, which is the adsorption peak caused by the lattice defect of carbon atoms, and the peak on the right is the G-band, which is the in-plane stretching vibration of the sp^2 hybridization of carbon atoms. The Raman spectra of Fig. 3C reveal that the C-LS adsorbent has D-band and G-band at 1,360 and 1,600 cm^{-1}, respectively. This indicates that there are sp^2 and sp^3 hybrid carbon atoms, and there are structural defects and oxygen-containing functional groups in C-LS. $I_D/I_G = 0.61$ obtained by calculation, can also be concluded that sodium lignosulfonate carbon spheres are amorphous

carbon, which is consistent with the XRD analysis results. Fig. 3C is the Raman spectrum of the C-LS adsorbent.

The dose of adsorbent directly affects the removal rate of metal ions and is also related to cost. It can be seen in Fig. 4A and B that the effect of the dose of adsorbent on the performance of the adsorbent. Overall, as the dose of adsorbent added increases, q_e decreases because the concentration of metal ions in the system is constant, the amount of adsorbent added increases, and only a small number of adsorption sites were utilized, resulting in the decrease of the average adsorption capacity of C-LS adsorbent. However, the removal rate of metal ions is also increasing until it approaches 100%. Based on these results, the subsequent adsorption experiment used 0.01 g of dose to conduct the adsorption experiment.

The effects of environmental conditions on the adsorption of Pb^{2+} and Cu^{2+} were studied due to the selective adsorptions of Pb^{2+} and Cu^{2+} on C-LS. The actual wastewater contains Na^+, K^+, Mg^{2+}, and Ca^{2+}, and they compete with heavy metals at adsorption sites of C-LS. In the experiment, three different concentration (0, 10, 100 mg L^{-1}) is set to explore the influence of those species on adsorption, which the concentration of Pb^{2+} and Cu^{2+} is 40 mg L^{-1}.
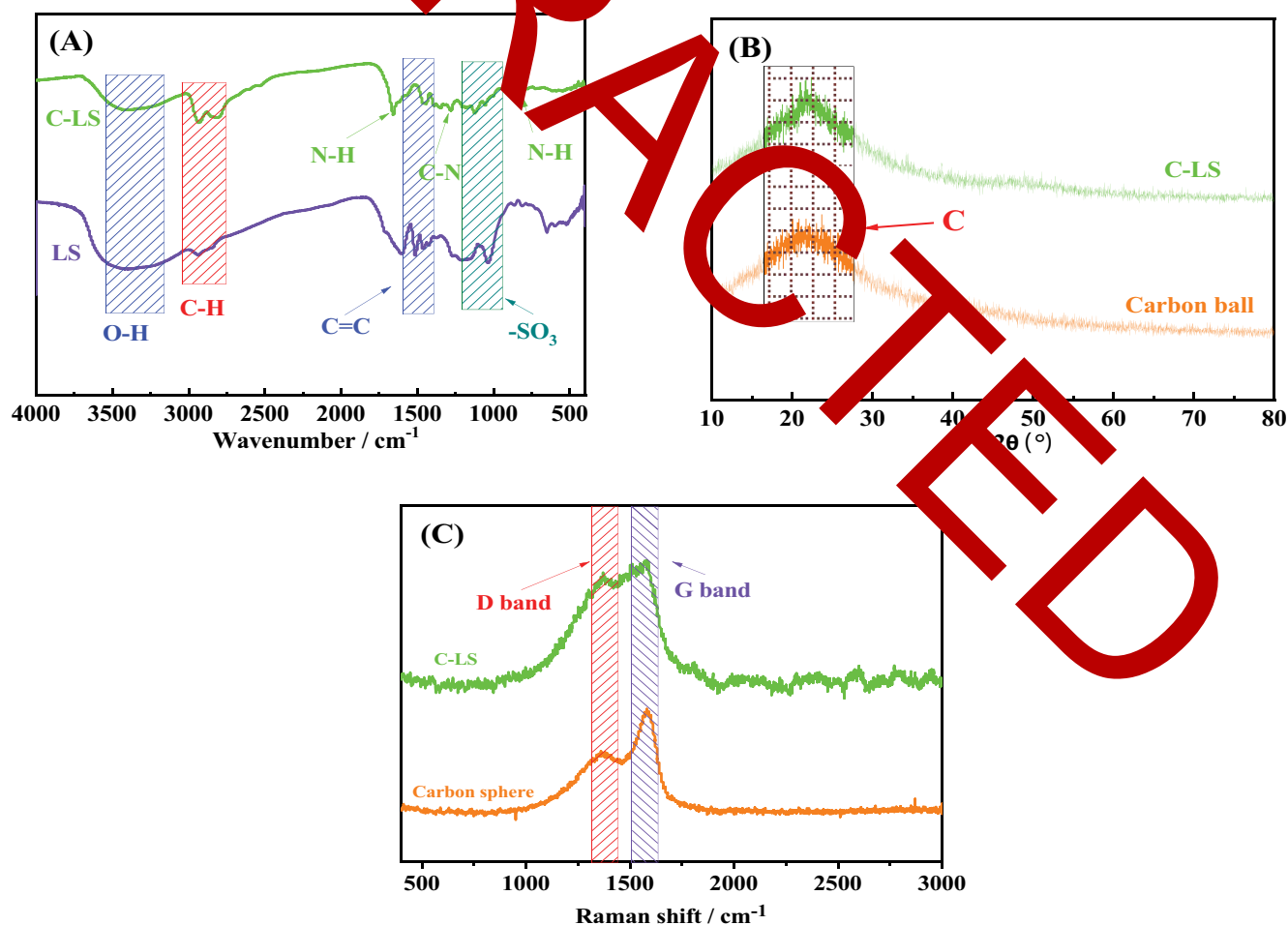
Fig. 3. Infrared spectra of sodium lignosulfonate (LS) and C-LS adsorbent (A), XRD patterns of hydrothermal carbon sphere and C-LS adsorbent (B), and Raman spectra of hydrothermal carbon spheres and C-LS adsorbent (C).
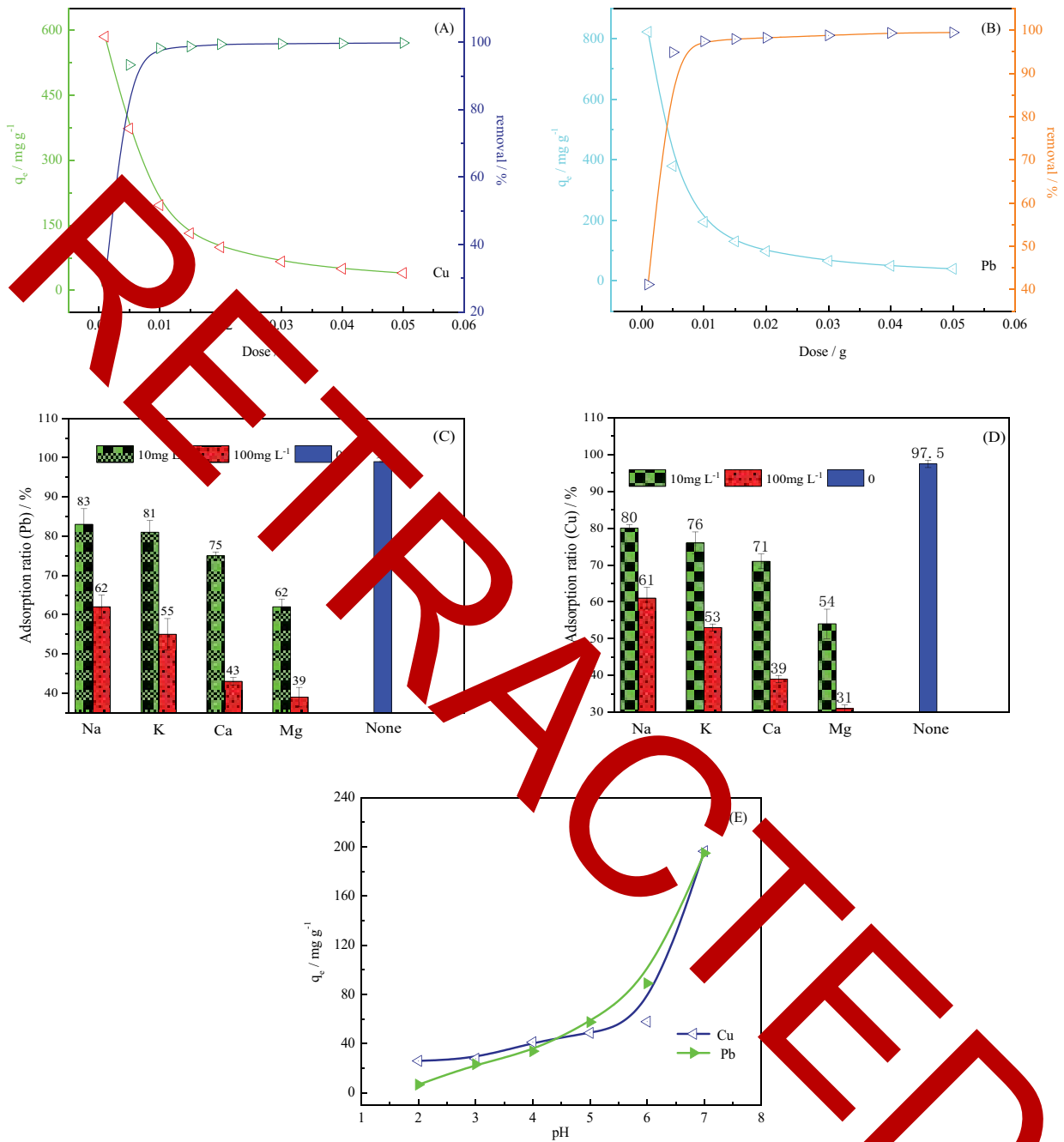
Fig. 4. Effect of the dose of C-LS adsorbent on the adsorption performance of C-LS adsorbent (A, B), the effect of different ions on adsorption performance of C-LS adsorbent (C, D) and effect of pH on the adsorption performance of C-LS adsorbent (E).

As shown in Fig. 4C and D, when the concentration of K^+, and Na^+ is 10 mg L^{-1}, the adsorption efficiency of Pb^{2+} and Cu^{2+} reaches 83% and 80%. When the concentration of K^+, and Na^+ is 100 mg L^{-1}, the adsorption efficiency of Pb^{2+} and Cu^{2+} have decreased by 25% and 23.8%. Furthermore, the effect of Ca^{2+} and Mg^{2+} on C-LS is obvious, especially Mg^{2+}. The order of influence of ion species is: $Mg^{2+} > Ca^{2+} > K^+ > Na^+$, which may be due to the difference in electronegativity. The reason for the decrease in adsorption efficiency may be the competition and electrostatic repulsion between

metal ions, and the decrease in the activity coefficients of Pb^{2+} and Cu^{2+} under high ionic strength [31].

pH is an important factor affecting the adsorbent. Since Cu^{2+} and Pb^{2+} will form hydroxide precipitates under alkaline conditions and affect the performance of the adsorbent, only neutral and acidic studies are done. It can be seen from Fig. 4E that the adsorption capacity of C-LS is greatly inhibited when pH is low. H^+ is more likely to combine with C-LS and occupy the adsorption site, which hinders the binding of C-LS with Cu^{2+} and Pb^{2+}. As the pH of
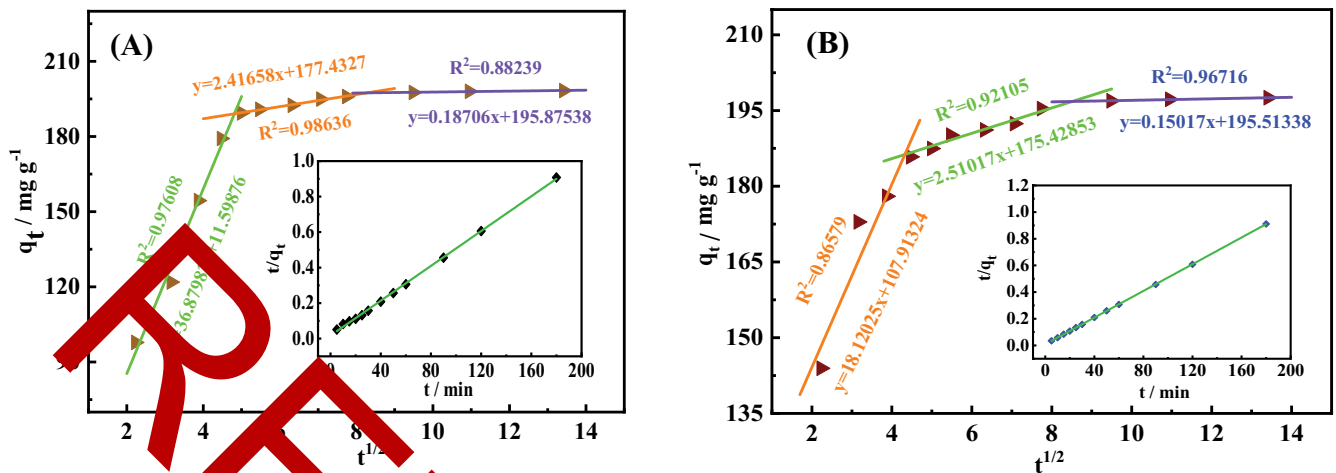
Fig. 5. Intraparticle diffusion model of C-LS adsorbent adsorb Cu^{2+} (Inset: pseudo-second-order) (A) and intraparticle diffusion of C-LS adsorbent adsorb Pb^{2+} (Inset: pseudo-second-order model) (B).

the solution increases, the inhibitory effect of Pb on C-LS decreases. There will be more adsorption sites on the surface of C-LS in solution occupied by heavy metal ions [3].

It can be seen from the graph of intraparticle diffusion in Fig. 5 that the adsorption process is segmented, with a rapid adsorption stage, a slow adsorption stage and an adsorption equilibrium stage. When the C-LS adsorbent is in contact with the metal ion solution, the metal ions quickly diffuse to the solid-liquid two-phase interface. At this time, the adsorption enters the rapid adsorption stage, and the adsorption rate is maximum; when metal ions reach the surface of C-LS adsorbent through the interface, the rate is slower than that of the first stage, so the overall adsorption rate decreases; when metal ions reach the surface of C-LS adsorbent, they combine with the adsorbent at the active sites, and the adsorption will reach equilibrium.

It can be seen from the illustrations in Fig. 5 that the pseudo-second-order kinetic data are basically on a line segment, and it is fitting correlation coefficient is closer to 1. Combined with the fitting parameters in Table 1, it is found that the difference between the adsorption capacity predicted by the pseudo-second-order kinetic data and the actual q_e is about 5%, while the error of the adsorption capacity predicted by the pseudo-first-order kinetic model is too large, it can be concluded that the phenomenon described by the pseudo-second-order kinetics model is closer to the experimental data. The adsorption process includes three process interface diffusion, adsorbent surface adsorption and adsorbent particle diffusion, which is also verified by the fitting results of intraparticle diffusion. The intraparticle diffusion shows that the adsorption rate of C-LS adsorbent is controlled by multiple processes, not by a single process [33–35].

It is known in Fig. 6A and B that the q_e of C-LS for heavy metal ions is concentration-dependent and increases with the increase of concentration at the same temperature, but it does not always increase. When the concentration exceeds 100 mg L^{-1}, the q_e does not increase any more, because the upper adsorption sites of C-LS are limited, so when they are fully occupied. When the temperature

Table 1
Kinetic models and parameters

Kinetic models and parameters		Cu^{2+}	Pb^{2+}
Actual	$q_{e,a}$ (mg g^{-1})	197	198
	q_e (mg g^{-1})	39.56	29.43
Pseudo-first-order	k_1 (min^{-1})	0.036	0.035
	R^2	0.866	0.955
	q_e (mg g^{-1})	207.6	201.6
Pseudo-second-order	k_2 (g mg^{-1} min^{-1})	0.0013	0.003
	R^2	0.999	0.999
	k_{p1} (mg g^{-1} min$^{-1/2}$)	36.88	18.12
	C_1	11.6	107.9
	R^2	0.9635	0.8534
	k_{p2} (mg g^{-1} min$^{-1/2}$)	2.351	2.51
Intraparticle diffusion	C_2	177.4	175.4
	R^2	0.9786	0.9121
	k_{p3} (mg g^{-1} min$^{-1/2}$)	0.1869	0.1511
	C_3	195.9	195.5
	R^2	0.8824	0.9672

rises, the adsorption capacity increases, which is due to the increase of active sites, which can combine with more metal ions.

A study of the Langmuir and Freundlich isotherm models reveals that the adsorption process is closest to the Langmuir isotherm process. It can be seen from Table 2 that the data points of the Langmuir isotherm model are concentrated on a line segment, the correlation coefficient is close to 1 and the predicted adsorption capacity is also close to the actual adsorption capacity. Compared with the Freundlich isotherm model, the correlation coefficient is small, and the predicted adsorption capacity differs greatly from the actual adsorption capacity of C-LS adsorbent. So, the adsorption process is the chemical adsorption of the monolayer described with the Langmuir isotherm model [36,37].
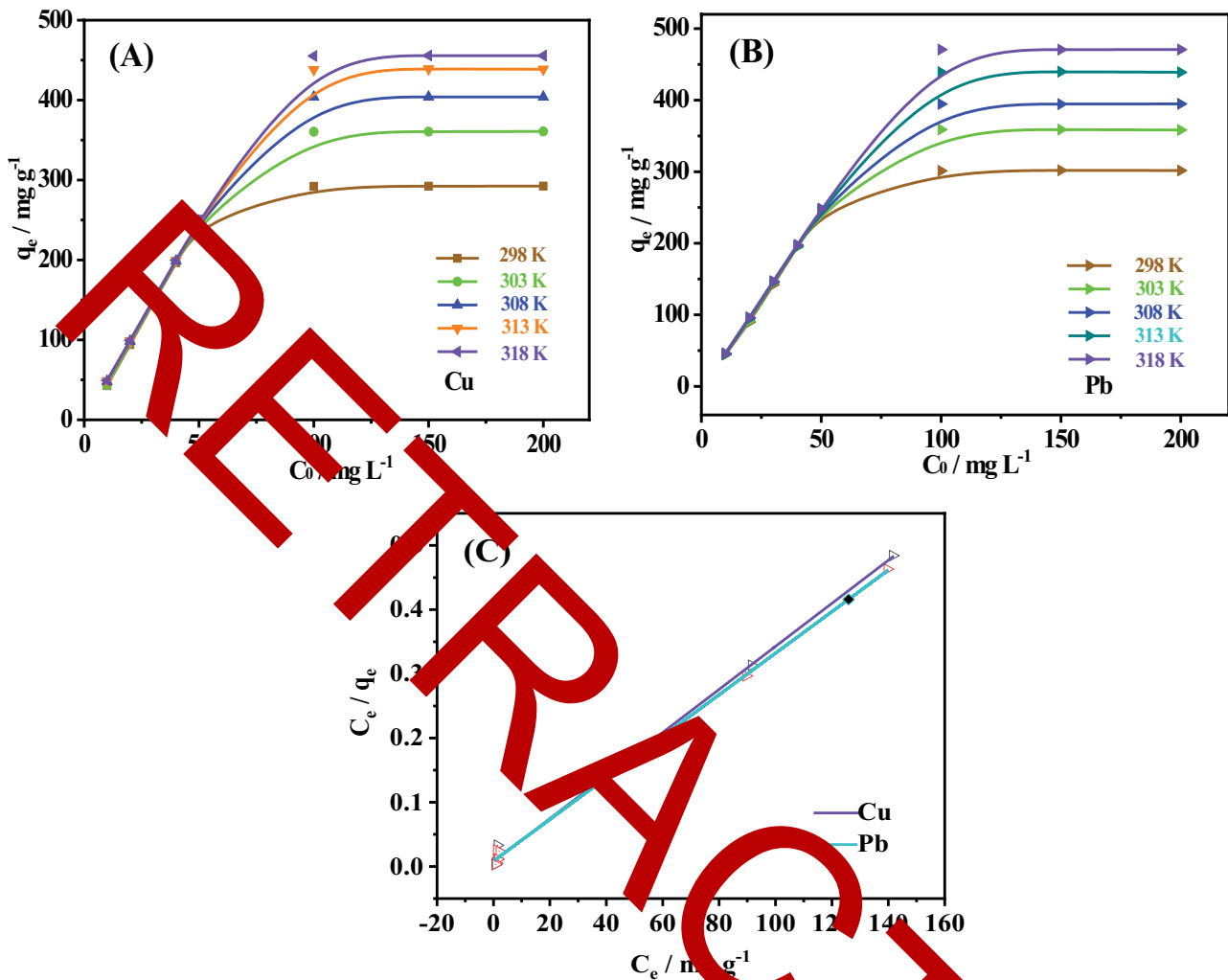
Fig. 6. Effect of different temperature on the adsorption performance of C-LS adsorbent (A, B) and the fitting of Langmuir isotherm model (C).

Table 2
Langmuir and Freundlich isotherm models parameter

Parameters		Cu²⁺					Pb²⁺				
		298 K	303 K	308 K	313 K	318 K	298 K	303 K	308 K	313 K	318 K
Langmuir	$q_{m,L}$ (mg g⁻¹)	289.6	360.1	397.4	431.5	465.5	299.5	360.1	39	440.5	72.2
	K_L (L mg⁻¹)	0.437	0.397	1.279	1.948	3.054	0.369	0.347	0.389	0.422	0.468
	R^2	0.996	0.992	0.998	0.997	0.999	0.996	0.995	0.994		0.998
Freundlich	K_F (L g⁻¹)	122.3	130.9	164.3	184.3	202.7	116.1	121.3	129.6	139.2	156.3
	$1/n$	0.181	0.198	0.202	0.196	0.181	0.201	0.242	0.253	0.282	0.263
	R^2	0.302	0.356	0.451	0.461	0.442	0.301	0.403	0.411	0.432	0.365

It can be seen from Fig. 6 that with the increase of temperature, the surface-active sites of C-LS adsorbent will increase, and resulting in the adsorption capacity of C-LS adsorbent will increase. In order to further explore the relationship between temperature and adsorption, the thermodynamic method was used to explore the adsorption heat.

The thermodynamic formula is used to fit the data, as shown in Fig. 7A, and Table 3 lists the results of thermodynamic fitting parameters. In Table 3, the entropy change $\Delta S°$ of adsorption is more than zero, which indicates that the entropy value increases in this process; the enthalpy change $\Delta H°$ of adsorption is more than zero, which indicates

that the whole adsorption process is endothermic; Gibb's function is calculated according to the enthalpy change and entropy change, and $\Delta G°$ is less than zero, which indicates that the adsorption process is a spontaneous process.

After the C-LS adsorbent adsorbs metal ions, add HCl to desorb the adsorbent, filter and dry, and then conduct the second adsorption experiment. After 5 adsorption experiments, it was found that the C-LS adsorbent still has high adsorption performance. The adsorption efficiency of the adsorbent for the two ions is not less than 84%. Simultaneously, it is revealed in Fig. 7B that the adsorption efficiency of C-LS adsorbent for Cu^{2+} and Pb^{2+} ions are basically the same,

indicating that C-LS adsorbent has no specificity for the adsorption of two ions.

It is necessary to carry out selective adsorption experiments to evaluate the absorptive capacity of target heavy metals. The main heavy metal ions in this study were Pb^{2+}, Cu^{2+}, Cd^{2+}, Zn^{2+} and Mn^{2+}, and adsorbed selectively. Fig. 7C shows the selective adsorption of these divalent heavy metal ions by C-LS at an initial concentration of 40 mg L^{-1}. The preferential adsorption rates of Pb^{2+} and Cu^{2+} ions were 89% and 81%, respectively. Sorption efficiency was ranked as Pb^{2+} > Cu^{2+} > Cd^{2+} > Mn^{2+} > Zn^{2+}. Adsorption selectivity may be due to differences in the electronegativity
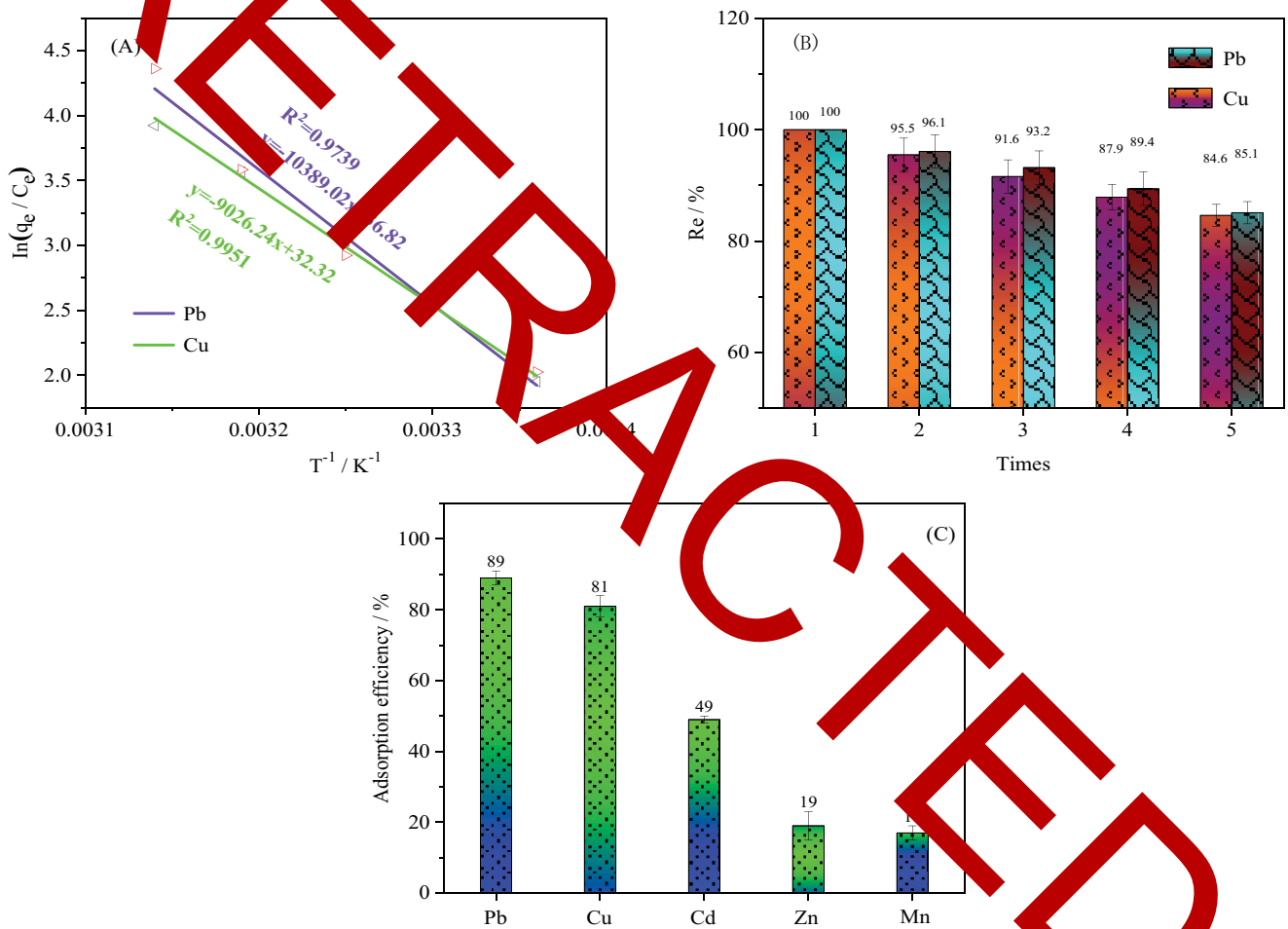
Fig. 7. Adsorption thermodynamics (A) and cycling efficiency of C-LS adsorbent multiple times (B), and C-LS selective adsorption of multiple ions (C).

Table 3
Thermodynamic parameter

T/K	Cu^{2+}					Pb^{2+}				
	298 K	303 K	308 K	313 K	318 K	298 K	303 K	308 K	313 K	318 K
$\Delta S°$/J mol^{-1} K^{-1}			281					305		
$\Delta H°$/kJ mol^{-1}			82					95		
$\Delta G°$/kJ mol^{-1}	–7.74	–9.14	–10.55	–11.95	–13.36	–5.89	–7.42	–8.94	–10.47	–11.99
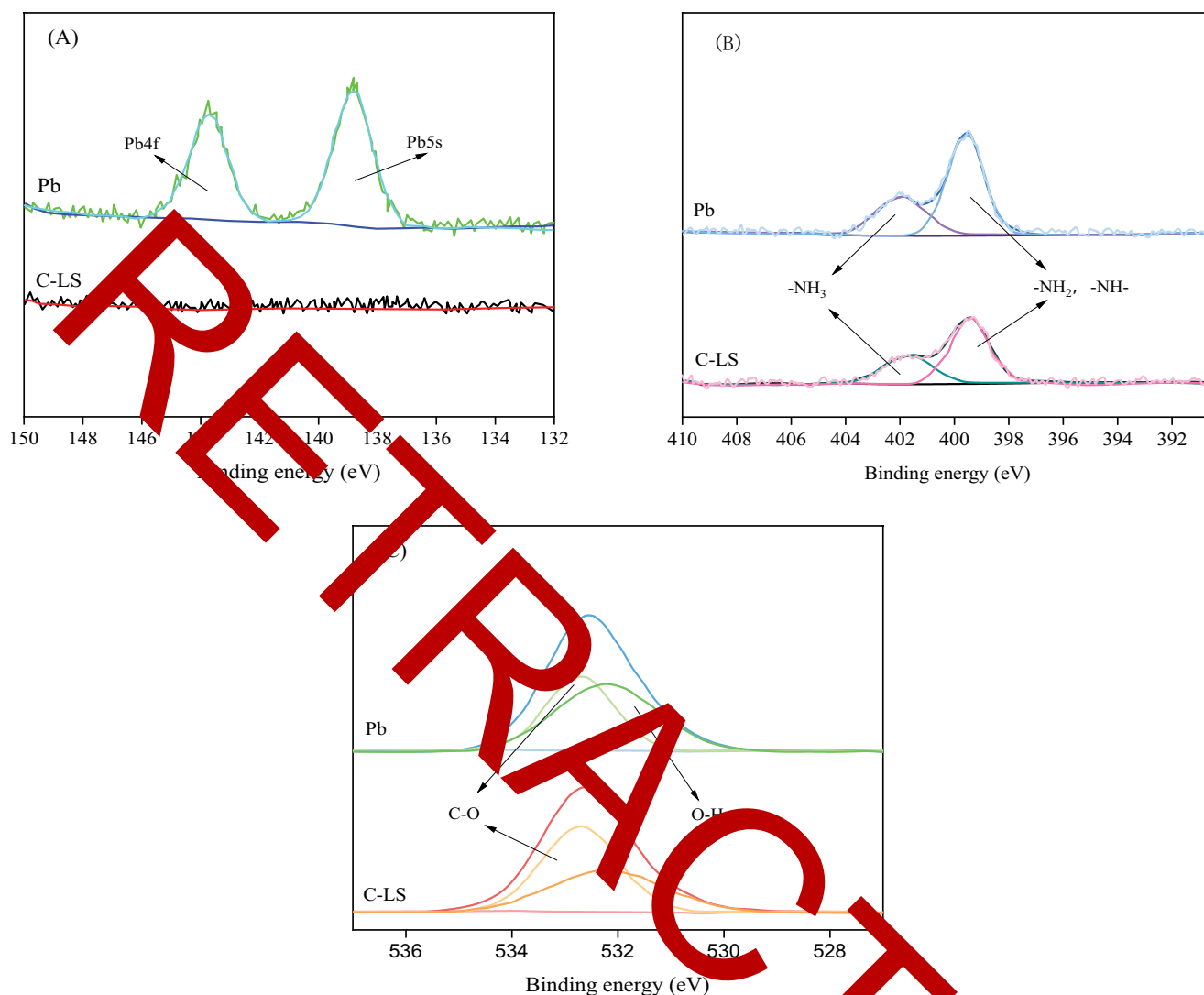
Fig. 8. Full-spectrum (A), N (B) and O (C) X-ray photoelectron spectra of C-LS before and after adsorption of Pb^{2+}.

of the metal ions (2.2 for Pb^{2+}, 1.90 for Cu^{2+}, 1.69 for Cd^{2+}, 1.65 for Zn^{2+}, 1.55 for Mn^{2+}) and the charge mass (103 for Pb^{2+}, 56 for Cd^{2+}, 32 for Cu^{2+}, 33 for Zn^{2+} and 27 for Mn^{2+}), as well as the ability to chelate the functional groups [38].

In order to investigate Pb^{2+} removal mechanism in detail, X-ray photoelectron spectroscopy was performed to study the change of chemical state before and after Pb^{2+} adsorption. As shown in Fig. 8A, there were no obvious peaks in C-LS, while Pb 5s and Pb 4f peaks appeared in the Pb spectra of C-LS-Pb, indicating that Pb^{2+} adsorption indeed occurred on the surface of C-LS, resulting in changes in the local bonding environment [39]. From the N spectra before and after Pb^{2+} adsorption (as shown in Fig. 8B), the peaks corresponding to $-NH_3$ and $-NH_2$, $-NH-$ of C-LS had a chemical shift after adsorption of Pb^{2+}, suggesting that the $-NH_3$ and $-NH_2$, $-NH-$ on the surface of C-LS were chemically bonded with Pb^{2+}. Furthermore, as shown in Fig. 6C, after adsorbing Pb^{2+}, the binding energy of O1s changed from 532.17 eV (C-LS) to 532.78 eV (C-LS-Pb) [40,41]. These results all indicated that O element

participated in the adsorption of Pb^{2+}. The O atom contained a pair of lone pairs of electrons, while the transition metals had empty atomic orbitals. They could share electrons to form amino-metal complexes.

4. Conclusion

In this work, the carbon spheres was synthesized by hydrothermal method and then combined with lignosulfonate to form a carbon-lignosulfonate (C-LS) adsorbent. C-LS has high adsorption efficiency for Cu^{2+} and Pb^{2+}, and 0.01g C-LS almost completely removed 40 mg L^{-1} of Cu^{2+} and Pb^{2+} solution. The process described by pseudo-second-order kinetics and Langmuir isothermal model is more consistent with the adsorption of Pb^{2+} and Cu^{2+} by C-LS, which also reveals that this process is chemisorption of the monolayer. In addition, it is found that the adsorption of Cu^{2+} and Pb^{2+} by C-LS is a spontaneous endothermic process. Simultaneously, after 5 adsorption–desorption experiments, C-LS still maintains more than 80% adsorption efficiency.

Data availability statement

The raw/processed data required to reproduce these findings cannot be shared at this time as the data also forms part of an ongoing study.

References

[1] S.W. Lee, S. Sarp, D.J. Jeon, J.H. Kim, Smart water grid: the future water management platform, Desal. Water Treat., 55 (2015) 339–346.

[2] Z. Dong, F. Zhang, D. Wang, X. Liu, J. Jin, Polydopamine-mediated surface-functionalization of graphene oxide for heavy metal ions removal, J. Solid State Chem., 224 (2015) 88–93.

[3] X. Liu, D.J. Lee, Thermodynamic parameters for adsorption equilibrium of heavy metals and dyes from wastewaters, Bioresour. Technol., 160 (2014) 24–31.

[4] N. Maalouf, P. Ortiz, M. Rendueles, A. Ghorbal, M. Díaz, Novel biosorbent from almond shells: characterization and adsorption properties modeling for Cu(II) ions from aqueous solutions, J. Environ. Chem. Eng., 5 (2017) 2944–2954.

[5] Y. Kuang, Y. Gao, F. Zhang, J. Zhao, G. Guo, D. Zhang, C. Lu, Y. Sun, Effect of initial pH on the sludge fermentation performance enhanced by aged refuse at low temperature of 10°C, Environ. Sci. Pollut. Res., 27 (2020) 31468–31478.

[6] R. Wang, W. Wang, H. Ren, J. Chae, Detection of copper ions in drinking water using the competitive adsorption of proteins, Biosens. Bioelectron., 57 (2014) 179–185.

[7] N.P. Raval, P.U. Shah, N.K. Shah, N. Shah, Adsorptive removal of nickel(II) ions from aqueous environment: a review, J. Environ. Manage., 179 (2016) 1–20.

[8] A.S. Singha, A. Guleria, Chemical modification of cellulosic biopolymer and its use in removal of heavy metal ions from wastewater, Int. J. Biol. Macromol., 67 (2014) 409–417.

[9] X.L. Liu, H.W. Pang, X.W. Liu, Q. Li, N. Zhang, L. Mao, M.Q. Qiu, B.W. Hu, H. Yang, X.K. Wang, Orderly porous covalent organic frameworks-based materials: superior adsorbents for pollutants removal from aqueous solutions, The Innovation, 2 (2021) 100076, doi: 10.1016/j.xinn.2021.100076.

[10] M. Šæiban, M. Klašnja, B. Škrbiæ, Adsorption of copper ions from water by modified agricultural by-products, Desalination, 229 (2008) 170–180.

[11] G.M. Zeng, J. Wan, D.L. Huang, L. Hu, C. Huang, M. Cheng, W.J. Xue, X.M. Gong, R.Z. Wang, D.N. Jiang, Precipitation, adsorption and rhizosphere effect: the mechanisms for phosphate-induced Pb immobilization in soils—a review, J. Hazard. Mater., 339 (2017) 354–367.

[12] M.J. Hao, M.Q. Qiu, H. Yang, B.W. Hu, X.X. Wang, Recent advances on preparation and environmental applications of MOF-derived carbons in catalysis, Sci. Total Environ., 760 (2021) 143333, doi: 10.1016/j.scitotenv.2020.143333.

[13] S.M. Zhu, N. Yang, D. Zhang, Poly(N,N-dimethylaminoethyl methacrylate) modification of activated carbon for copper ions removal, Mater. Chem. Phys., 113 (2009) 784–789.

[14] M. Imamoglu, M. Tekir, Removal of copper(II) and lead(II) ions from aqueous solutions by adsorption on activated carbon from a new precursor hazelnut husks, Desalination, 228 (2008) 108–113.

[15] Y.H. Li, S.G. Wang, A.Y. Cao, D. Zhao, X.F. Zhang, C.L. Xu, Z.K. Luan, D.B. Ruan, J. Liang, D.H. Wu, B.Q. Wei, Adsorption of fluoride from water by amorphous alumina supported on carbon nanotubes, Chem. Phys. Lett., 350 (2001) 412–416.

[16] X.H. Wang, Y.Y. Wang, S.F. He, H.Q. Hou, C. Hao, Ultrasonic-assisted synthesis of superabsorbent hydrogels based on sodium lignosulfonate and their adsorption properties for Ni²⁺, Ultrason. Sonochem., 40 (2018) 221–229.

[17] Y. Fu, X. Liu, G. Chen, Adsorption of heavy metal sewage on nano-materials such as titanate/TiO₂ added lignin, Results Phys., 12 (2019) 405–411.

[18] A.T. Xie, J.D. Dai, X. Chen, P. Ma, J.S. He, C.X. Li, Z.P. Zhou, Y.S. Yan, Ultrahigh adsorption of typical antibiotics onto novel hierarchical porous carbons derived from renewable lignin via halloysite nanotubes-template and in-situ activation, Chem. Eng. J., 304 (2016) 609–620.

[19] X. Wang, Y. Wang, H. Hou, J. Wang, H. Chen, Ultrasonic method to synthesize glucan-g-poly(acrylic acid)/sodium lignosulfonate hydrogels and studies of their adsorption of Cu²⁺ from aqueous solution, ACS Sustainable Chem. Eng., 5 (2017) 6438–6446.

[20] T.Q. Zhao, K. Zhang, J.W. Chen, X.B. Shi, X. Li, Y.L. Ma, G.Z. Fang, S.Y. Xu, Changes in heavy metal mobility and availability in contaminated wet-land soil remediated using lignin-based poly(acrylic acid), J. Hazard. Mater., 368 (2019) 459–467.

[21] Y.C. Zhang, S.Z. Ni, X.J. Wang, W.H. Zhang, L. Lagerquist, M.H. Qin, S. Willför, C.L. Xu, P. Fatehi, Ultrafast adsorption of heavy metal ions onto functionalized lignin-based hybrid magnetic nanoparticles, Chem. Eng. J., 372 (2019) 82–91.

[22] Y. Meng, J. Lu, Y. Cheng, Q. Li, H.S. Wang, Lignin-based hydrogels: a review of preparation, properties, and application, Int. J. Biol. Macromol., 135 (2019) 1006–1019.

[23] J.Z. Ma, M.A. Khan, M.Z. Xia, C.L. Fu, S.D. Zhu, Y.T. Chu, W. Lei, F.Y. Wang, Effective adsorption of heavy metal ions by sodium lignosulfonate reformed montmorillonite, Int. J. Biol. Macromol., 138 (2019) 188–197.

[24] M.Y. Liu, Y. Liu, J.J. Shen, S.Y. Zhang, X.Y. Liu, X.X. Chen, Y.L. Ma, S.X. Ren, G.Z. Fang, S.J. Li, C.T. Li, T. Sun, Simultaneous removal of Pb²⁺, Cu²⁺ and Cu²⁺ ions from wastewater using hierarchical porous polyacrylic acid grafted with lignin, J. Hazard. Mater., 392 (2020) 122208, doi: 10.1016/j.jhazmat.2020.122208.

[25] B. Ibrahim, M. Schlegel, N. Kanswohl, Investigation of applicability of wetland biomass for producing biochar by hydrothermal carbonization (HTC), Landbauforschung-Ger. Appl. Agric. For. Res., 64 (2014) 119–124.

[26] N. Brun, K. Sakaushi, L. Yu, L. Giebeler, J. Eckert, M.M. Titirici, Hydrothermal carbon-based nanostructured hollow spheres as electrode materials for high-power lithium-sulfur batteries, Phys. Chem. Chem. Phys., 15 (2013) 6080–6087.

[27] M. Sevilla, A.B. Fuertes, The production of carbon materials by hydrothermal carbonization of cellulose, Carbon, 47 (2009) 2281–2289.

[28] C. Baccile, G. Laurent, F. Babonneau, F. Fayon, M. Titirici, M. Antonietti, Structural characterization of hydrothermal carbon spheres by advanced solid-state MAS 13C NMR investigations, J. Phys. Chem. C, 113 (2009) 9644–9654.

[29] A. Fiori, D. Basso, D. Castello, M. Baratieri, Hydrothermal carbonization of biomass: design of a batch reactor and preliminary experimental results, Chem. Eng. Trans., 37 (2014) 55–60.

[30] J. Yang, A. Sudik, C. Wolverton, D.J. Siegel, High capacity hydrogen storage materials: attributes for automotive applications and techniques for materials discovery, Chem. Soc. Rev., 39 (2010) 656–675.

[31] Y.Y. Wang, L.L. Zhang, X.H. Wang, W.R. Zheng, C. Hao, C.L. Jiang, J.B. Wu, Synthesis of aminated calcium lignosulfonate and its adsorption properties for azo dyes, Ind. Eng. Chem., 61 (2018) 321–330.

[32] C. Jiang, X. Wang, B. Hou, C. Hao, X. Wu, Construction of a lignosulfonate–lysine hydrogel for the adsorption of heavy metal ions, J. Agric. Food Chem., 68 (2020) 3050–3060.

[33] C. Jiang, X. Wang, D. Qin, W. Da, B. Hou, C. Hao, J. Wu, Construction of magnetic lignin-based adsorbent and its adsorption properties for dyes, J. Hazard. Mater., 369 (2019) 50–61.

[34] A. Etaati, S. Pather, Z. Fang, H. Wang, The study of fibre/matrix bond strength in short hemp polypropylene composites from dynamic mechanical analysis, Composites, Part B, 62 (2014) 19–28.

[35] H. Zhou, H. Zhu, F. Xue, H. He, S. Wang, Cellulose-based amphoteric adsorbent for the complete removal of low-level heavy metal ions via a specialization and cooperation mechanism, Chem. Eng. J., 385 (2020) 123879, doi: 10.1016/j.cej.2019.123879.

[36] Y. Zhu, W. Fan, T. Zhou, X. Li, Removal of chelated heavy metals from aqueous solution: a review of current methods and mechanisms, Sci. Total Environ., 678 (2019) 253–266.

[37] Q. Huang, D. Hu, M. Chen, C. Bao, X. Jin, Sequential removal of aniline and heavy metal ions by jute fiber biosorbents: a practical design of modifying adsorbent with reactive adsorbate, J. Mol. Liq., 285 (2019) 288–298.

[38] L. Xia, Y. Lu, H. Meng, C. Li, Preparation of C-MOx nanocomposite for efficient adsorption of heavy metal ions via mechanochemical reaction of CaC_2 and transitional metal oxides, J. Hazard. Mater., 393 (2020) 122487, doi: 10.1016/j.jhazmat.2020.122487.

[39] Y. Liu, T. Xiao, P.C. Baveye, J. Zhu, Z. Ning, H. Li, Potential health risk areas with high naturally-occurring cadmium background in southwestern China, Ecotoxicol. Environ. Saf., 112 (2015) 122–131.

[40] Z. Lin, Y. Hu, Y. Yuan, B. Hu, B. Wang, Comparative analysis of kinetics and mechanisms for Pb(II) sorption onto three kinds of microplastics, Ecotoxicol. Environ. Saf., 208 (2021) 111451, doi: 10.1016/j.ecoenv.2020.111451.

[41] B. Wang, Y. Li, J. Zheng, Y. Hu, B. Hu, Efficient removal of U(VI) from aqueous solutions using the magnetic biochar derived from the biomass of a bloom-forming cyanobacterium (*Microcystis aeruginosa*), Chemosphere, 254 (2020) 126898, doi: 10.1016/j.chemosphere.2020.126898.